

NISTIR 6439

**REDUCED-SCALE EXPERIMENTS TO
CHARACTERIZE THE SUPPRESSION
OF RACK-STORAGE COMMODITY
FIRES**

**Anthony Hamins
Kevin McGrattan**

**Building and Fire Research Laboratory
Gaithersburg, MD 20899**

NIST

**United States Department of Commerce
Technology Administration
National Institute of Standards and Technology**

NISTIR 6439

**REDUCED-SCALE EXPERIMENTS TO
CHARACTERIZE THE SUPPRESSION
OF RACK-STORAGE COMMODITY
FIRES**

**Anthony Hamins
Kevin McGrattan**

**Building and Fire Research Laboratory
National Institute of Standards and Technology
Gaithersburg, MD 20899**

November 1999



U.S. Department of Commerce
William M. Daley, *Secretary*
Technology Administration
Dr. Cheryl L. Shavers, *Under Secretary of Commerce for Technology*
National Institute of Standards and Technology
Raymond G. Kammer, *Director*

Abstract

A series of reduced-scale experiments were conducted to investigate the burning and water suppression of rack-storage commodity fires. The objective of the research reported here is to support the NIST Fire Dynamics Simulator (FDS), a computational fluid dynamics model that endeavors to predict fire growth, spread, sprinkler activation, and suppression by water in rack-storage commodity fires. The model requires appropriate and implementable sub-grid algorithms that adequately represent the full-scale heat and mass transfer that occurs in a warehouse fire with rack-storage of standard commodities. In particular, this report describes experiments that investigated the effect of water application on the time required to achieve ignition of the unburned commodity and on the heat release rate of the burning commodity.

Several types of experiments were conducted. These include ignition measurements using the LIFT apparatus and the cone calorimeter, and heat release rate measurements using oxygen consumption calorimetry. All of these measurements were made with and without water application. The data were analyzed using algorithms that were appropriate and readily implementable in the FDS. A description of the experimental apparatus and procedures precedes a description of the experimental results.

1. Introduction

This report describes a number of reduced-scale experiments supporting the development of the NIST computational fire model known as the Fire Dynamics Simulator (FDS). The FDS is a computational fluid dynamics (CFD) model that calculates fire growth and spread in a large enclosure. A central challenge for the FDS model is to represent fire phenomena like ignition, flame spread, and water suppression in a way that preserves what is known about the underlying physics, but is tractable computationally. The objective of the work described here is to provide measurements from appropriate reduced-scale experiments that can be used within the various fire related FDS sub-models.

An overview of the FDS calculation scheme is shown in Fig. 1. Fire growth is a process that couples gas phase heat release and condensed phase mass loss in a positive feedback loop. The model includes convective and radiative heat transfer to the fuel surface. Ignition is achieved when the surface temperature exceeds a prescribed threshold. Once ignition is achieved, Lagrangian particles, here referred to as thermal elements, are emitted from the fuel surface and release heat at a prescribed rate. The thermal elements generate a buoyancy-induced flow field, which in turn transports the elements. The energy released by a thermal element is partitioned into convective and radiative components. The convective component heats the gas, and the radiative component heats surrounding surfaces. The total heat release rate of the fire is the sum of the heat release rates of the thermal elements. Sprinklers are activated mainly by convective heat transfer from the buoyant hot gases. In the model, water from a sprinkler impacts both ignition and the local heat release rate (denoted as \dot{q}'' in Fig. 1). These interactions are the focus of this investigation. In particular, we quantify the effect of water application on (1) the time required to achieve ignition of the unburned commodity and (2) the heat release rate of the burning commodity.

The spatial resolution of the model is limited by the size of the domain and the calculation time. For the application of interest, a single cell of the computational grid is on the order of 10 cm. Phenomena that occur at smaller scales cannot be modeled directly, but must be described through sub-models and empirical correlations. The FDS model requires information on the thermal properties of the fuel, including the ignition temperature, and the local burning rate with and without water application. It is preferable to obtain this information from experiment rather than through more detailed sub-models because it saves on computational costs, minimizes the propagation of compound errors, and because the underlying physics is not well understood. A detailed discussion of the thermal element model and its application to fire phenomena can be found in McGrattan et al. [1998a; b]. Details regarding the FDS computational scheme as applied to the rack-storage problem can be found in the companion reports [2000a; b].

The remainder of this report is broken into a number of sections. Section 2 describes the commodity in some detail including the thermal and flammability properties of its components. Section 3 describes ignition measurements using the LIFT device and the cone calorimeter. Section 4 describes heat release rate measurements using oxygen consumption calorimetry on the individual components of the commodity (polystyrene, and corrugated paper) and on a single cell within the commodity. Section 5 describes experiments designed to measure the effective radiative fraction of the fire. Section 6 describes experiments to measure the speed of water

flowing over vertical surfaces of the commodity. Section 7 considers the ignition of wet corrugated paper. Section 8 describes the effect of water on the heat release rate of the commodity. The experimental apparatus, procedure, and results are described in each section. Section 9 consists of a brief summary of our findings. Acknowledgements and references are cited at the end of the report.

2. Group A Plastic Commodity

The fuel selected for testing was the Group A Plastic Commodity*, obtained from Underwriters Laboratories [Sheppard, 1998]. The fire protection industry commonly uses this fuel to test the effectiveness of water sprinklers and other fire protection devices [Sheppard, 1998]. It is a multi-component fuel composed of compartmentalized unexpanded polystyrene cups in corrugated paper cartons. Eight cartons loaded on a wood pallet comprise one pallet-load of the Commodity. Each carton is 0.53 m wide by 0.53 m deep by 0.53 m high. Vertical and horizontal cardboard dividers are used to form the

125 cells in a 5 x 5 x 5 array. Within each cell is one polystyrene cup. Each cup weighs 36 g and has a 0.45 L capacity. Table 1 lists the mass and the exposed surface area of the constituents of one (conditioned) palette of the commodity obtained from Underwriter Laboratories (UL). The uncertainty listed in Table 1 is an estimate of the combined standard uncertainty (σ), which is dominated by instrument reading accuracy. The mass of the constituents of the Group A Commodity reported by Factory Mutual (Yu et al., 1994) differs by as much as 20% from the values shown in Table 1. All materials used in the experiments described in this report were obtained from UL. Table 1 shows that the corrugated paper has the largest exposed surface of the pallet components, and its burning dominates the early fire behavior. Observation indicates that first the outer shell burns and that soon thereafter, the polystyrene cups become involved. They begin to deform and eventually ignite. Subsequently, the cups melt and drip, and burning proceeds to the next cell.

Component	Mass (kg)	Exposed Surface (m ²)	Exposed Vertical Surface in Flue (m ²)
Corrugated Paper: Shell	8±0.4	5±0.1	1±0.05
Corrugated Paper: Internal	12±0.4	0	0
Polystyrene Cups	36±0.1	0	0
Wood Pallet	24±1	0.5±0.02	0.1±0.01
Total	80±1.9	5.5±0.1	1.1±0.06

* Certain trade names and company products are mentioned in the text to specify adequately the experimental procedure and equipment used or to identify types of currently available commercial products. In no case does such identification imply recommendation or endorsement by the National Institute of Standards and Technology, nor does it imply that the products are necessarily the best available for the purpose.

Because the cartons are constructed of corrugated paper, their burning behavior is affected by the directionality of the corrugation. The thickness of the corrugated paper sheet is approximately 4 mm, although observation indicates that it is often compressed to as little as 1 mm. For all experiments with the sheet oriented in a vertical direction, the direction of the ribs or flues was maintained vertically, as is the case for the sides of the manufactured box.

3. Ignition

Flame spread along the surface of the carton is controlled by the local incident heat flux and the thermal properties of the corrugated paper. A search of the fire literature indicates that information on the ignition of corrugated paper has not been previously documented. In any case, the thermal properties of one type of corrugated paper may be very different than other types, due to differences in physical properties such as its internal structure.

Apparatus and Procedure

The time to sustained flaming was measured using a sample of the outer shell of the commodity oriented in a vertical configuration in the LIFT apparatus. The LIFT test and apparatus has been described in detail previously [ASTM E 1321]. Similar experiments were conducted using the cone calorimeter [ASTM E 1354]. Standard test methods were used. As in all experiments, the samples were conditioned before testing at standard conditions: 50% relative humidity and a temperature of 20° C. The incident heat flux at the sample surface was measured with a total heat flux gauge and allowed to equilibrate to a steady value. Unless otherwise noted, a small pilot flame or electric spark was used as an ignition source. The sample was placed in front of the radiant source, covered by a thick marine board. The board was removed and the time to sustained flaming was measured using a stopwatch.

Results and Discussion

As the conditioned sample of corrugated paper was exposed to an incident flux, it became darker until a black char layer formed on the surface. Figure 2 shows results from the LIFT experiments for the time to flaming ignition as a function of the incident heat flux. Figure 2 shows that the time to ignition increased as the incident flux decreased until a critical flux was obtained below which sustained flaming was not obtained. For flux levels less than 14 kW/m², the sample smoldered, but flaming ignition did not occur before the entire sample smoldered away. For flux levels less than 20 kW/m², the sample first smoldered and only later was a sustained flame observed. Unfortunately, flux levels in the LIFT device are limited. For moderate to high flux levels (>40 kW/m²), the cone calorimeter was used.

During observation of small, moderate and full-scale experiments using the Plastic A Commodity, a large number of flaming brands were observed. This implies that the normal mechanism for ignition in the warehouse fires of interest is piloted, although non-piloted ignition could occur for example during the phenomena of aisle jumping in an actual warehouse fire. To study the effect of the pilot flame on ignition, a number of non-piloted ignition experiments were also conducted in the LIFT. Figure 2 shows that non-piloted ignition required significantly

longer preheat times than piloted ignition. In this study, piloted ignition is assumed to be representative of the warehouse fire problem.

Figure 3 shows the reciprocal of the time to ignition as a function of the external flux for the same data as shown in Fig. 2. The critical flux (\dot{q}_{crit}'') is found by fitting a straight line to the data and noting at what flux the time to ignition becomes infinite. [Ohlemiller and Villa, 1991]. From Fig. 3, the critical flux was determined to be approximately 14.5 kW/m². This value was then used to characterize the thermal properties of the corrugated paper sample. In Figure 4, the ratio of the critical flux to the external flux is plotted as a function of the time to ignition. Such a plot allows interpretation of a sample's flammability parameters in terms of a thermally thin analysis [Ohlemiller and Villa, 1991]. A fit to the data in the form shown in Fig. 4 yields an exponential term whose coefficient is equal to the ratio of an effective heat transfer coefficient, h , to the lumped thermal parameter, $c_p \rho \delta$, which is the product of the effective specific heat, density, and thickness of the material. Using the methodology outlined by Ohlemiller and Villa [1991], the ignition temperature was estimated as 370°C and the value of h was estimated as 0.042 kW/m²-K. Heat flux measurements during moderate-scale fire tests indicate that fluxes as high as 90 kW/m² to 110 kW/m² occur on the vertical box surfaces. Therefore, in Fig. 4, only data for fluxes greater than 40 kW/m² were used to determine $c_p \rho \delta$, leading to a value of 0.98 kJ/m²-K. The results in Fig. 4 show that the high flux data are adequately fit using this approach. Treatment of the material as thermally thick also yields an adequate fit, but for reasons of computational efficiency and simplicity, the thermally-thin approach was used.

4. Heat Release Rate of a Single Cell and its Components

A series of reduced-scale experiments was undertaken to characterize the effective caloric value of a single cell from the commodity and its constituents. The cone calorimeter was used to determine the effective heat of combustion of samples of the polystyrene cup, corrugated paper, and a single cell sample of the Group A Plastic Commodity. A cell consisted of a single polystyrene cup surrounded on six sides by corrugated paper. These experiments yield insight into the burning character of the commodity at full-scale, which is composed of multiple cells (see Section 2 for a description of the commodity).

In a calorimeter, the measured or actual heat release rate (\dot{Q}_m'') is equal to the product of the mass burning rate (\dot{m}) and the evolved heat per unit mass of fuel (H_m). The parameter H_m is also known as the effective heat of combustion. It should be noted that the measured heat release rate is not equal to the product of the mass burning rate, \dot{m} (in units of kg/s), and the idealized heat of combustion per unit mass of fuel, H_c (in units of MJ/kg).

$$\begin{aligned} \dot{Q}_m'' &= \dot{m} H_m \\ &\neq \dot{m} H_c \end{aligned} \quad (1)$$

These parameters are related, however, through the combustion efficiency (χ_a), which is defined as the ratio of H_m to H_c :

$$\chi_a = H_m/H_c = \dot{Q}_m'' / \dot{m} H_c \quad (2)$$

The value of χ_a cannot be directly measured, but it can be inferred through knowledge of H_c , measurements of \dot{Q}_m'' and \dot{m} , and use of Eq. 2. The value of H_c is known for pure fuels (see Table 3) and can be calculated for multicomponent fuels where the relative mass percentages are known, such as for the commodity (see below).

Apparatus and Procedure

The cone calorimeter has been described in detail previously [ASTM E 1354]. Three types of samples were tested. In the first experiment, a flat circular piece (5 cm diameter) of polystyrene (PS) extracted from the bottom of a single polystyrene cup was placed in a standard holder and mounted horizontally in the cone calorimeter. In the second experiment, a flat square piece of conditioned corrugated paper (10 cm x 10 cm) was positioned in a manner similar to the PS. In the third experiment, a single inverted (bottom-side up) polystyrene cup was placed within a corrugated paper cell (10cm x 10 cm x 10 cm). This cube was placed within a metal housing that had only the front face open. A 10 mm gap was provided between the paper sides of the cell and the metal housing. The front surface of the cell was placed at the standard distance (2.5 cm) from the cone heater (which was positioned vertically).

The heat release rate of the burning cell measured in the cone calorimeter cannot be extrapolated to large-scale (multiple cells stacked vertically). This is because the large-scale local environment of a single cell cannot be simulated using the cone calorimeter. For example, during the single cell experiments in the cone calorimeter, the external flux was incident only onto the front face of the sample. While this arrangement may adequately represent the early burning behavior of the outer cell at full-scale, at later times, convective and radiative heating from below will influence the full-scale burning. A further limitation of a single cell cone calorimeter experiment is that the applied flux on the sample is too low. Full-scale experiments in two, three and four tier configurations showed that the heat flux on the vertical surfaces of the cardboard boxes was typically 90 kW/m² to 110 kW/m². The inconel heater in the NIST cone calorimeter is restricted to a maximum flux of 75 kW/m².

Table 2 lists the mass, mass percent, and the heat of combustion per unit mass of oxygen consumed (H_c/r_o) for a single box of the commodity and its constituents. The parameter H_c was defined above and r_o is the mass-based stoichiometric ratio of fuel to air. For the calculation of the heat release rates, the value of H_c/r_o was assumed to be a constant throughout the experiment, with a value equal to 13.46 MJ/(kg of O₂ consumed). This represents an average of the mass-weighted values of polystyrene and corrugated paper (see Table 2). This value is only slightly different (<3%) from the value of 13.1 MJ/kg of O₂ assigned typically to uncharacterized fuels. The uncertainty listed in Table 2 is an estimate of the combined standard uncertainty (σ), which is dominated by instrument reading accuracy.

Table 2. Mass, Mass Percent, and Heat Release Rate per Mass of Oxygen for Components of a Single Box of the Commodity.

Component	Mass (kg)	Mass Percent	H_c/r_o^B (MJ/kg of O ₂)
Corrugated Paper	2.5±0.1 ^A	36±1	13.19 ^C
Polystyrene Cups	4.5±0.01	64±1	13.61
Average per box	7.0±0.1	100	13.46

A. Measurements in bold.
 B. Babrauskas, 1997.
 C. Data for cellulose [Babrauskas, 1997] - data not available for corrugated paper.

Results and Discussion

Figure 5 shows the measured heat release rate during two experiments, when single cells of Group A Plastic Commodity were burned in the cone calorimeter. The results in the figure indicate that the measurements were reproducible until ~150 s, with larger variations thereafter. The combined standard uncertainty (2σ) in the heat release rate is approximately $\pm 5\%$ based on previous studies [Enright and Fleishman, 1999]. Differences in the curves in Fig. 5 are attributed to the stochastic nature of fire phenomena. In Fig. 5, the corrugated paper ignited after approximately 10 s of exposure to the 50 kW/m² incident flux. As the front face burned, the heat release rate rose rapidly. After the front face burned away, the corrugated paper sides of the box began to burn and the PS cup began to melt. The presence of the PS cup moderated the burning process, shielding the rear portions of the cell from exposure to radiative flux. After approximately 40 s, the PS cup ignited and started to burn. Large amounts of smoke and radiation were then emitted by the fire. The heat release rate increased, leveled-off, and then gradually decreased. Typically, several grams of PS (from the cup) dripped over the metal frame in fine strands and large drips. Figure 6 shows the effective heat of combustion ($\chi_a H_c$ or H_m), for the same data as shown in Fig. 5. The data in Fig. 6 are consistent with the description of the burning process of the Group A Plastic Commodity. The value of $\chi_a H_c$ was initially small (10 MJ/kg to 15 MJ/kg), which is characteristic of the burning of corrugated paper (see Table 3). Later in the experiment, $\chi_a H_c$ increased to ~27 MJ/kg, a value between the H_c values for PS and corrugated paper listed in Table 3.

Table 3. Heat of Combustion of the Constituents of the Commodity.

Component	H_c^A (MJ/kg)	$\chi_a H_c$ (MJ/kg)	χ_a
Corrugated Paper	17 ^B	14±2	0.82±0.12
Polystyrene Cups	40	26±2	0.65±0.05
Average per box	32	23±2	0.71±0.06

A. Babrauskas, 1997.
 B. Data for cellulose; data is not available for corrugated paper.

The cone calorimeter results for burning of PS and corrugated paper are summarized in Table 3, which lists the values of H_c taken from the literature, the measured effective heat of combustion ($\chi_a H_c$), and estimates of χ_a determined by dividing the latter by the former. Because H_c values for corrugated paper are not available, data for cellulose was used, as listed in Table 3. This is considered a reasonable approximation because paper products are mainly composed of cellulose. Estimates of χ_a for the box constituents were determined from the ratio of the measured effective heats of combustion ($\chi_a H_c$) to the literature values of H_c . The value of χ_a for PS is within 6% of that reported by Tewarson [1987]. The estimate of $\chi_a H_c$ in Table 3 for the Commodity was determined as a mass-based average of the results for the constituents. The uncertainty listed in Table 3 is an estimate of the combined standard uncertainty (2σ) based on repeat experiments and previous uncertainty analysis of heat release rate calculations in the cone calorimeter [Enright and Fleishman, 1999]. The total mass of one box of the Plastic Commodity is 7 kg (see Table 1). The results in Table 3 on $\chi_a H_c$ for each of the commodity's components imply that the total integrated heat release rate from one box of the commodity should be approximately 161 MJ. Eight boxes form a palette, so one palette of the commodity has a potential energy of ~1.3 GJ or a potential energy density of 1.1 GJ/m³.

5. Effective Radiative Fraction

The radiative loss fraction from a flame (χ_r) is defined as the ratio of the rate of radiative energy emitted to the surroundings (\dot{Q}_r), to the idealized heat release rate ($\dot{m} \cdot H_c$):

$$\chi_r = \dot{Q}_r / (\dot{m} \cdot H_c) \quad (3)$$

Substituting Eq. 2 into Eq. 3 leads to the following:

$$\chi_r = \chi_a \cdot \dot{Q}_r / \dot{Q}_m \quad (4)$$

where χ_a and \dot{Q}_m are defined in Section 4. We define an effective radiative fraction (χ_{ra}) as equal to the ratio of the radiative fraction and the combustion efficiency (χ_a):

$$\chi_{ra} = \chi_r / \chi_a = \dot{Q}_r / \dot{Q}_m \quad (5)$$

The value of χ_{ra} can be thought of as the ratio of the rate of radiative energy emitted to the actual heat release rate. This is exactly the input required by the FDS fire model, which explicitly partitions the actual heat release rate (\dot{Q}_m) between the rate of radiative energy loss (\dot{Q}_r) and the rate of sensible enthalpy convected by the fire plume (\dot{Q}_p). In other words, the sum of the rates of radiative and convected energy is the actual heat release rate (\dot{Q}_m):

$$\dot{Q}_m = \dot{Q}_r + \dot{Q}_p \quad (6)$$

An effective sensible enthalpy fraction (χ_{pa}) can be defined, which is equal to the ratio of the

enthalpy convected by the plume to the actual heat release rate:

$$\chi_{pa} = \dot{Q}_p / \dot{Q}_m \quad (7)$$

Dividing Eq. 6 by \dot{Q}_m leads to:

$$1 = \chi_{ra} + \chi_{pa} \quad (8)$$

Information regarding the combustion efficiency is not explicitly needed by the model. The value of χ_{ra} for the commodity was estimated by measuring \dot{Q}_r and \dot{Q}_m (see Eq. 5). The value of χ_{pa} was then calculated using Eq. 8.

Apparatus and Procedure

The radiative flux was measured using a single location measurement with total heat flux gauges [Hamins et al., 1991; Modak, 1977]. The gauges had a wide view angle (150°) and were coated with a thin layer of spectrally flat, high absorptivity paint. Figure 7 is a schematic drawing of the experimental set-up. Both gauges were positioned approximately 2.6 m (5 box lengths) away from the fire, beyond the footprint of the exhaust hood. This was done to avoid convective heat transfer to the gauges and to ensure that the assumption of an isotropic radiation field could be applied. The gauges were separated by 2 m with one of the gauges positioned directly in front of the box and the second located 45° away, as seen in Fig. 7. Both gauges were positioned 0.9 m above the ground. The gauges were calibrated using a high intensity lamp and a gauge traceable to NIST standards.

Four line-igniters were used to ignite all four sides of the corrugated box simultaneously as seen in Fig. 7. The igniters provided 0.8 (L/s) of propane, yielding an idealized heat release rate of 65 kW distributed about the four sides of the box. The flames engulfed the commodity and caused rapid ignition uniformly about the box. Several seconds after establishing the propane igniter flames, the flame height began to grow as the cartons began to burn. At the same time, the box surface blackened. The propane igniters were turned off 60 s after ignition. The experiment was terminated after 300 s.

Assuming isotropic radiation, the radiative flux from the fire to the surroundings was calculated as:

$$\dot{Q}_r = 4\pi R^2 \dot{q}_f'' \quad (9)$$

where \dot{q}_f'' is the radiative flux (kW/m²) measured at a distance R from the box center (2.6 m). The value of χ_{ra} was determined using Eq. 5. The actual heat release rate (\dot{Q}_m) was measured using oxygen consumption calorimetry in the NIST furniture calorimeter [ASTM E 1354].

Results and Discussion

Figure 8 shows the measured radiative loss (\dot{Q}_r) from the two radiometers and the measured heat release rate (\dot{Q}_m) during the first 300 s of burning of a single box of the Plastic Commodity. The combined standard uncertainty (2σ) in \dot{Q}_r is estimated as approximately $\pm 10\%$. As mentioned previously, the combined standard uncertainty (2σ) in \dot{Q}_m is approximately $\pm 5\%$. During the experiment shown in Fig. 8, the data acquisition system commenced to acquire background signal at 0 s. The propane igniter flames were initiated at 60 s and terminated 60 s later, 120 s into the measurement. The values of \dot{Q}_r (Eq. 5) calculated from the two radiometer measurements tracked each other very closely. Using Eq. 5 and averaging the \dot{Q}_r data in Fig. 8, the time varying values for χ_{ra} were determined and are shown in Fig. 9. The measurement of χ_{ra} was meaningful after 120 s, when the propane igniter flames were terminated. For early times in the experiment, before the PS cups ignite, the value of χ_{ra} is rather small (~ 0.2). As the cups burned more vigorously, the fire became more luminous and the value of χ_{ra} increased until it reached a value of nearly 0.44. Repeat experiments yielded nearly identical results. The combined standard uncertainty (2σ) in χ_{ra} is estimated as approximately $\pm 15\%$.

6. Water Flow on the Commodity

In this Section, the impact of water on the ignition and burning rate of the fuel is investigated. First, measurements were made on the speed of water sliding down a vertical surface. This is important information because the FDS model must track sprinkler droplets, both in the air and on the surface of the commodity.

Apparatus and Procedure

A 1.5 mm thick copper plate (25 cm wide by 35 cm long) was oriented vertically. A 9 mm diameter tube with 1 mm diameter holes every 1 cm was used to introduce the water flow into a triangular trough with an adjustable gap to assure uniform water application over the entire width of the plate. A cloth was periodically swept across the face of the plate, creating a uniform flow over the width of the plate. This was necessary because surface tension effects caused breakup of the water flow into rivulets after a period of 10 s to 20 s. The rate of water flowing down the vertical surface was controlled with a regulating valve. A small amount of water-soluble white dye was periodically added to the water flow by a spray bottle to increase contrast with the plate and facilitate tracking the water's descent. A video camera recorded the flow.

Results and Discussion

A series of volumetric flows was tested in the range from 7 ml/s to 23 ml/s. Figure 10 shows the measured water speed as a function of the volumetric water flow normalized by the width (25

cm) of the plate. The measurements showed that the average speed of the water along the vertical surface was approximately 0.54 m/s (± 0.03 m/s) with little influence of the total water flow on the speed.

7. Effect of Water on the Ignition of a Commodity

Apparatus and Procedure

The time to sustained flaming due to application of water on the exposed surface of a horizontally oriented corrugated paper sample was investigated using the cone calorimeter [ASTM E 1354]. The sample was positioned horizontally to promote uniform water evaporation and a uniform heat flux on the sample surface. The experiments were performed only in the cone calorimeter, because the LIFT device requires vertical orientation of the sample. The samples were conditioned before testing and the same standard test methods described in Section 3 were used.

The sample was weighed before water application. Water was applied with a small brush and allowed to soak into the sample for approximately two minutes. The sample mass was measured just before testing to avoid significant water evaporation. The sample and cover were placed in front of the radiant source and the time to ignition was measured after removing the cover.

Results

Figure 11 shows the results from experiments testing the effect of applied water in delaying the time to flaming ignition of the corrugated paper sample. The figure presents the ignition time as a function of the mass of water applied per unit area of cardboard for two incident fluxes: 20 kW/m² and 25 kW/m². In the figure, idealized behavior is indicated by the solid lines and was based on the assumptions that (1) the added water was completely evaporated before ignition and (2) the incident heat flux, water application, and evaporation were uniform over the sample surface. Figure 11 shows that the measured time to ignition appears to be adequately represented by the idealized behavior. In summary, application of water on an intact portion of the commodity can significantly delay or prevent ignition, depending on the incident heat flux and the water application flux.

8. Suppression by Water

Yu et al. [1994] performed a series of large-scale fire suppression tests for the commodity. They analyzed their results in terms of a global heat balance model, which assumed a form for the total fire heat release rate after water application as:

$$\dot{Q}(t) = \dot{Q}_o \cdot \exp[-k(t-t_o)] \quad (10)$$

where $\dot{Q}(t)$ is the total heat release rate following the application of water, \dot{Q}_o is the total heat release rate at the time of water application t_o , and k is a fire suppression parameter that is related

to the fuel density, fuel specific heat, ignition temperature, heat of combustion, total burning rate, heat of pyrolysis, and average water application rate. Yu et al. [1994] showed that the coefficient k can be correlated as a linear function of the water application rate for a particular period (240 s) from the time of water application. The values of k varied for the two types of commodities tested using Yu's model.

Unfortunately, Yu's model cannot be directly applied in the FDS calculation. Yu's model is a global suppression model that predicts the effect of the water application rate on the total heat release rate, but it does not predict the local heat release rate, nor the heat release rate without water application. The FDS model requires a burning rate algorithm applicable to all times, with and without water. This information is provided by the reduced-scale experiments described below. Although Yu's model (Eq. 10) is not directly applicable to the FDS methodology, we seek a functional form for the local heat release that is analogous to Eq. 10, which relates the local heat release rate with the local water application rate. It was originally hoped that this could be achieved using information from experiments using single or multi-cell samples of the Group A Plastic Commodity in the cone calorimeter or a mini-furniture calorimeter (50 kW maximum), but as discussed earlier, those experiments do not adequately replicate the local thermal environment of a single cell within the full-scale burning commodity. Thus, a larger scale experiment was designed.

Apparatus and Procedure

The experiments were performed at Underwriters Laboratories. In total, 19 experiments were conducted. The entire fuel/nozzle arrangement was located below a large exhaust hood that was instrumented to measure the heat release rate using oxygen consumption calorimetry [ASTM E 1354]. The methodology is appropriate for a burning sample undergoing water suppression [Dlugogorski, 1994].

The fuel and nozzle arrangement used in these experiments is shown in Fig. 12. It consisted of four boxes of the commodity. The boxes were stacked two high. The two stacks were positioned 15 cm from each other, creating a flue that had the same separation as that used in the full-scale tests. A water applicator was positioned above the boxes to deliver a uniform water flux directly on top of the boxes. The applicator was supported such that its four nozzles were 30 cm above the tops of the boxes. Four nozzles were positioned symmetrically about the center of the flue. The nozzles were arranged on the corners of a square with 0.6 m sides, providing water coverage of a 1.49 m² area. The nozzles were connected to a 8 cm diameter water line that was insulated by approximately 1 cm of ceramic fiber insulation. Several nozzle sizes were used, depending on the desired water flux. Table 4 lists the average water application flux (\dot{M}_{wf}'') and the time of water application. The water application time was varied from 30 s to 200 s, whereas the water flux was varied from 0.03 kg/m²-s to 0.66 kg/m²-s. These flux values covered the full range of interest. For example, Yu et al. [1994] found that water suppression was achieved with a flux of 0.077 kg/m²-s, 0.108 kg/m²-s, and 0.139 kg/m²-s in two, three, and four tier fires burning the commodity, respectively.

Table 4. Time and Rate of Water Application.

Experiment No.	Application Time (s)	Total Water Flow		Average Water Application Flux	
		(kg/s)	(gpm)	(kg/m ² -s)	(gpm/ft ²)
1	380	0.98	15.5	0.66	0.97
2	470	0.57	9.0	0.38	0.56
3	65	0.41	6.5	0.28	0.41
4	106	0.41	6.5	0.28	0.41
5	115	0.11	1.8	0.074	0.11
6	122	0.11	1.8	0.074	0.11
7	150	0.079	1.3	0.053	0.08
8	93	0.11	1.8	0.074	0.11
9	93	0.21	3.3	0.14	0.20
10	110	0.21	3.3	0.14	0.20
11	205	21	3.3	0.14	0.20
12	116	0.16	2.5	0.11	0.16
13	63	0.16	2.5	0.11	0.16
14	64	0.28	4.5	0.19	0.28
15	71	0.079	1.3	0.053	0.08
16	62	0.047	0.9	0.032	0.05
17	104	0.047	0.9	0.032	0.05
18	58	0.079	1.3	0.053	0.08
19	30	0.079	1.3	0.053	0.08

The ignition source was a propane igniter that consisted of two parallel 12.5 mm diameter copper tubes each 30 cm long. The two tubes were joined by a tee at one end. The tubes were separated by a 12.5 cm gap. Along the top of each tube, 1 mm diameter holes were drilled every 1 cm. A small torch was used to ignite the igniter, which was turned on at time zero and turned off 30 s later. The propane flow through the igniter was approximately 0.5 L/s, yielding a 40 kW fire that was nearly 50 cm in height. The igniter flames entirely covered the vertical sides of the boxes in the flue space. The Commodity rapidly ignited (~5 s) and the flames rapidly grew, reaching nearly 1.5 m just 10 s after ignition.

Results and Discussion

The heat release rate results of the suppression experiments for Tests 1-19 are shown in Fig. 13. As expected, the heat release rates were very similar from test to test for the first 30 s of burning. The heat release rates decreased at the time of water application (see Table 4). After an initial rapid decrease at the time of water application, the heat release rates often increased slowly with time. This behavior occurred somewhat in Tests 8, 9, 10, and 16, and more prominently in Tests 13-15 and 17-19. In these experiments, either small water fluxes were applied or the application times were relatively late in the experiment

The heat release rate measurements are well-fit by the following functional form:

$$\dot{q}''(t) = \dot{q}_o''(t) \cdot [(\exp(k_1[t-t_0])) + k_2[t-t_0]] \quad (11)$$

where $\dot{q}''(t)$ is the local heat release rate per unit area, $\dot{q}_o''(t)$ is the heat release rate per unit area without water application, and k_1 and k_2 are the local suppression coefficients (s^{-1}), which are equal to zero for $t \leq t_0$. As in Eq. 10, t_0 is the time of water application. The form of Eq. 11 is similar to the form of Yu's correlation (Eq. 10), except there is an additional term involving k_2 , which represents the observation that $\dot{q}''(t)$ slowly increased with time after an initial rapid decrease in the heat release rate.

The results of Tests 1 and 2 are shown in Fig. 14. In these tests, the water was not applied until very late in the experiments (> 400 s). These results were used to define the profile of $\dot{q}_o''(t)$, which is the basis for all conclusions regarding the effect of the applied water flux. For that reason, the data was smoothed. A constant value was used to represent \dot{q}_o'' for times greater than 400 s, as indicated by the line in Fig. 14. Following Yu et al., k_1 is taken as proportional to the water application rate:

$$k_1 = a_1 M_w'' \quad (12)$$

where a_1 is a constant ($m^2/kg\cdot s$) and M_w'' is the average water application mass per unit exposed area of the commodity surface (kg/m^2). The value of M_w'' is defined as:

$$M_w'' = \dot{M}_{wf}'' \cdot A / U \cdot P \quad (13)$$

where \dot{M}_{wf}'' is the average water flux at the box tops ($kg/m^2\cdot s$), A is the surface area of a single box top ($0.28 m^2$), U is a reference speed ($0.54 m/s$) taken as the water cascade speed (see Section 6 above), and P is the perimeter along the top of a single box unit ($2.12 m$). The average water flux (\dot{M}_{wf}'') is listed in Table 4 for each of the experiments. When M_w'' is equal to zero, \dot{q}'' is equal to \dot{q}_o'' . Figure 15 shows the normalized heat release rates (\dot{q}'' / \dot{q}_o'') for a number of the experiments, indicating that the form of Eq. 11 is appropriate. The other experiments are equally well-fit. Figure 16 shows the value of k_1 as a function of the water application rate (M_w''). From the figure, the best-fit value for a_1 (Eq. 12) is found to be approximately -1.0 . The value of a_1 is negative, because the water application decreased the heat release rate.

The value of k_2 (s^{-1}) was also related to the water application rate. Figure 17 shows k_2 as a function of the water mass per unit area for all of the experiments listed in Table 4. A straight line fit to the data yields:

$$k_2 = a_2 M_w'' + b_2 \quad (14)$$

The values of a_2 and b_2 are equal to $-0.020 \text{ m}^2/\text{kg}\cdot\text{s}$ and 0.0015 s^{-1} , respectively, determined by the best-fit line shown in Fig. 17. When $t \leq t_0$, then the values of the constants k_2 , a_2 , and b_2 are defined as zero, insuring that \dot{q}'' is equal to \dot{q}''_0 in Eq. 11.

The functional form of Eq. 11 is appropriate for characterizing the heat release rate in the Fire Dynamics Simulator. In the analysis, however, the water flux was assumed to be uniform. In Tests 1-19, however, the water density was not uniform, but varied spatially. For this reason, the coefficients in Eqs. 12 and 14 may need modification when implemented in the Fire Dynamics Simulator, which is discussed in detail by McGrattan et al. [2000a;b].

9. Summary

A series of experiments was conducted to characterize the suppression of rack-storage commodity fires burning the Group A Plastic Commodity. This work provides information that adequately quantifies a number of important mass and heat transfer processes that occur in a rack storage fire involving the Group A Plastic Commodity. The information derived here will be used in the Fire Dynamics Simulator to predict the growth and suppression of a full-scale rack storage fire [McGrattan, 2000a;b]. Details of that model can be found in McGrattan et al. [2000a;b]. The efficacy of the results presented here should be judged in terms of the success of that model in simulating the fire growth, spread, and water suppression in full-scale rack-storage experiments.

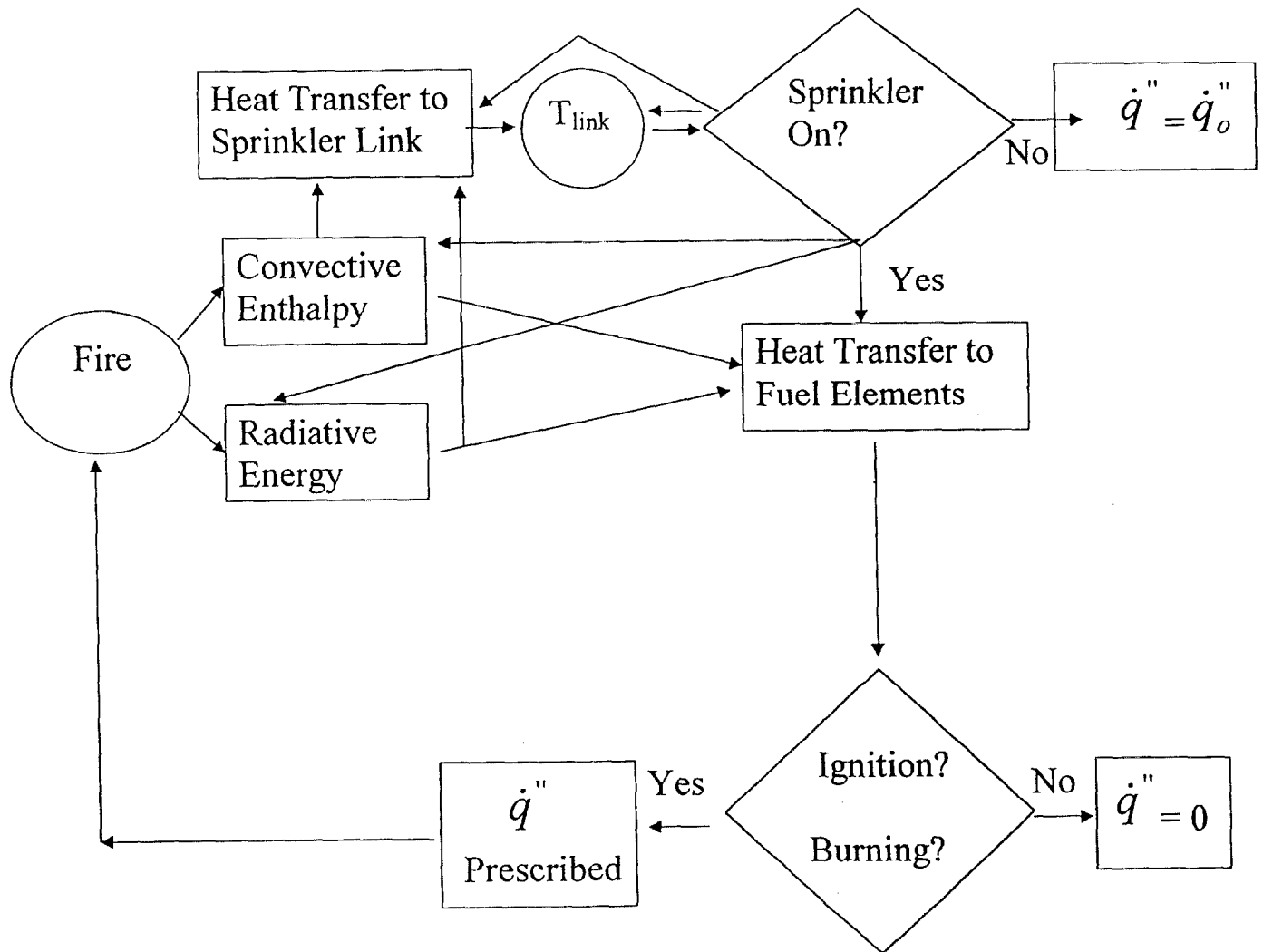
10. Acknowledgements

Thanks are due to Steve DeGiovanni of the University of Maryland and Dr. Jukka Hietaniemi of VTT Building Technology, Finland for many helpful discussions and for assistance with some of the measurements. The authors are also grateful to Lauren DeLauter, Gary Rodarmel, Roy McLane, Randy Shields, and Michael Smith of NIST and Dave Sheppard of U.L. for assistance with the measurements.

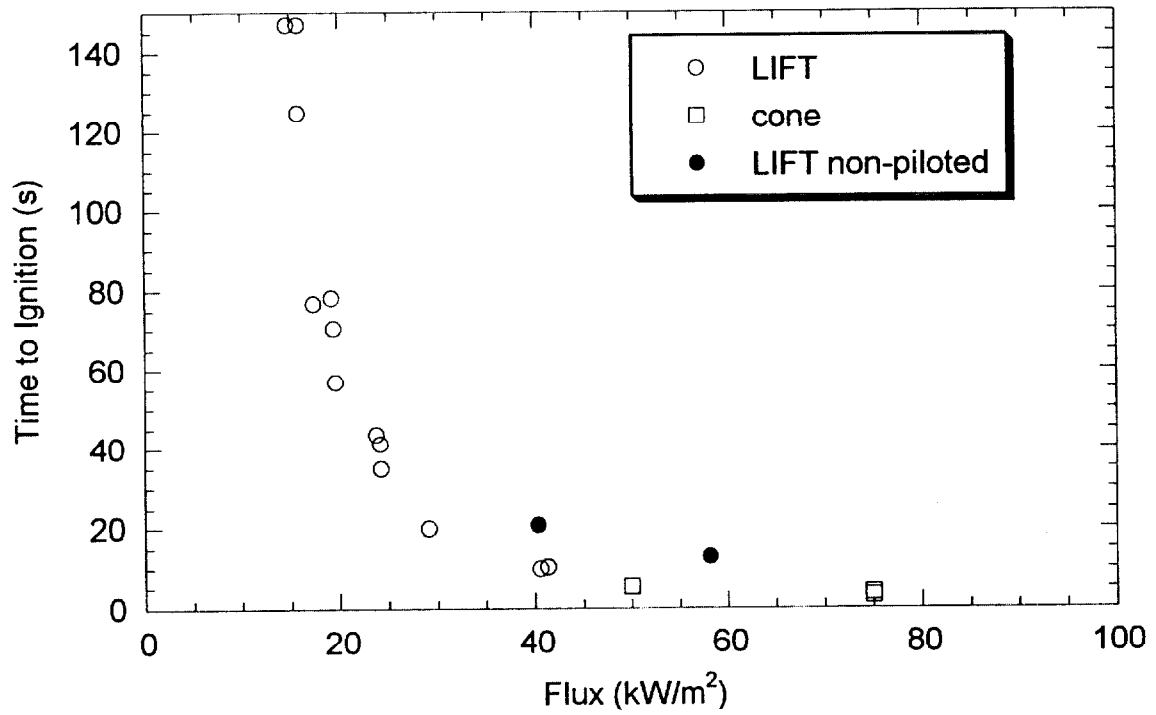
11. References

- ASTM E-1321-90, *Standard Test Method for Determining Material Ignition and Flame Spread Properties*, American Society for Testing and Materials, Philadelphia, PA, 1990.
- ASTM E-1354-94, *Standard Test Method for Heat and Visible Smoke Release for Materials and Products Using an Oxygen Consumption Calorimeter*, American Society for Testing and Materials, Philadelphia, PA, 1994.
- Babrauskas, V., *Appendix A*, Fire Protection Handbook (Ed.: A. Cote), 18th edition, National Fire Protection Association, Quincy MA, 1997.
- Dlugogorski, B.Z., Mawhinney, J.R., and Duc, V.H., *Proc. 4th Int. Sym. on Fire Safety Science*, 877-888, 1994.
- Enright, P.A. and Fleishman, C.M., *Fire Tech.*, 35, 153-169 (1999).
- Hamins, A., Kashiwagi, T., Gore, J., and Klassen, M., *Combust. Flame*, 86, 229-236, (1991).
- McGrattan, K., Baum, H.R., Rehm, R.G., *Fire Safety Journal*, 30, 161-178 (1998a).
- McGrattan, K., Hamins, A., Stroup, D., *Sprinkler, Smoke, Heat Vent, Draft Curtain Interaction – Large Scale Experiments and Model Development*, NIST Technical Report NISTIR 6196-1, National Institute of Standards and Technology, Gaithersburg, MD, 1998b.
- McGrattan, K., Baum, H.R., Rehm, R.G., Hamins, A., and Forney, G.P., *Fire Dynamics Simulator-Technical Reference Manual*, NIST Internal Report NISTIR 6467, National Institute of Standards and Technology, Gaithersburg, MD, January 2000a.
- McGrattan, K., and Forney, G.P., *Fire Dynamics Simulator-User's Manual*, NIST Internal Report NISTIR 6469, National Institute of Standards and Technology, Gaithersburg, MD, January 2000b.
- Modak, A., *Combust. Flame*, 29, 177-192 (1977).
- Ohlemiller, T.J., and Villa, K.M., *Material Flammability Test Assessment for the Space Station Freedom*, Technical Report NISTIR 4591, National Institute of Standards and Technology, Gaithersburg, MD 20899, 1991.
- Sheppard, D.T., *Heptane Burner Tests and Commodity Tests*, International Fire Sprinkler, Heat & Smoke Vent, Draft Curtain, Fire Test Project, National Fire Protection Research Foundation (NFPRF) Technical Report, Batterymarch Park, Quincy, MA, April 1998.
- Tewarson, A., *Prediction of Fire Properties of Materials*, National Bureau of Standards Report # NBS-GCR-86-521, December 1986.

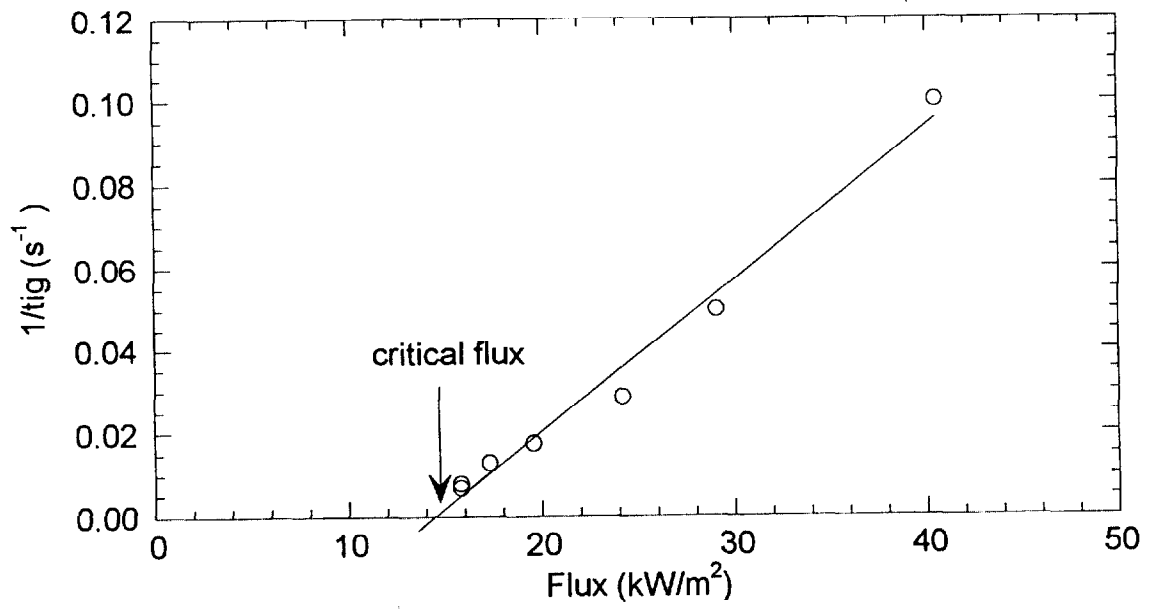
Yu, H.Z., Lee, J.L., Kung, H.C., *Proc. 4th Int. Sym. on Fire Safety Science*, 901-912, 1994.



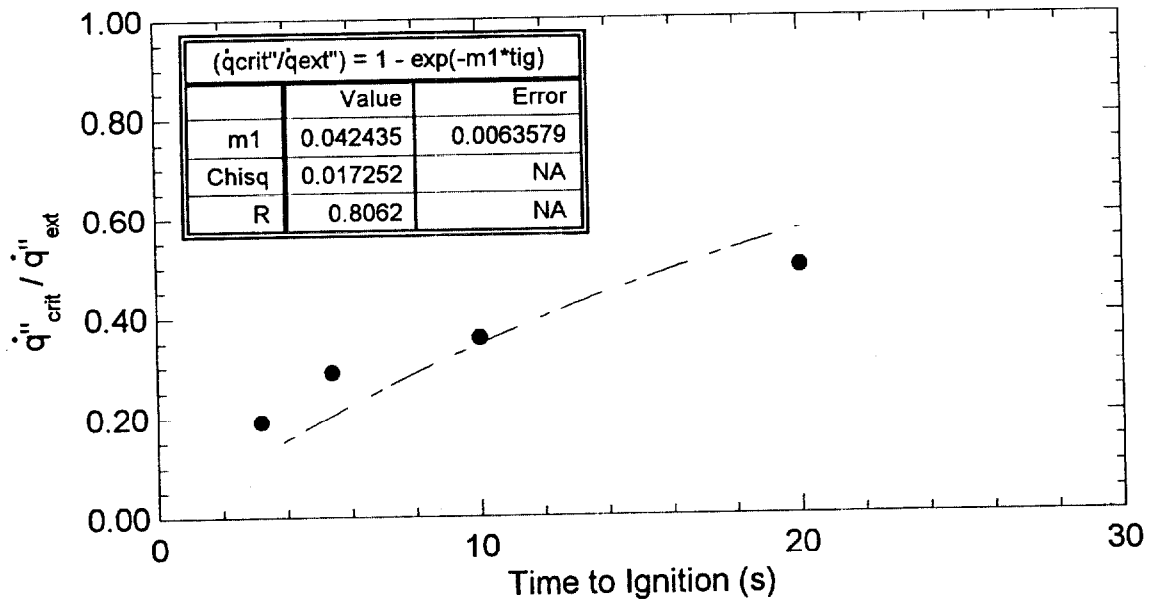
1. An overview of the calculation scheme.



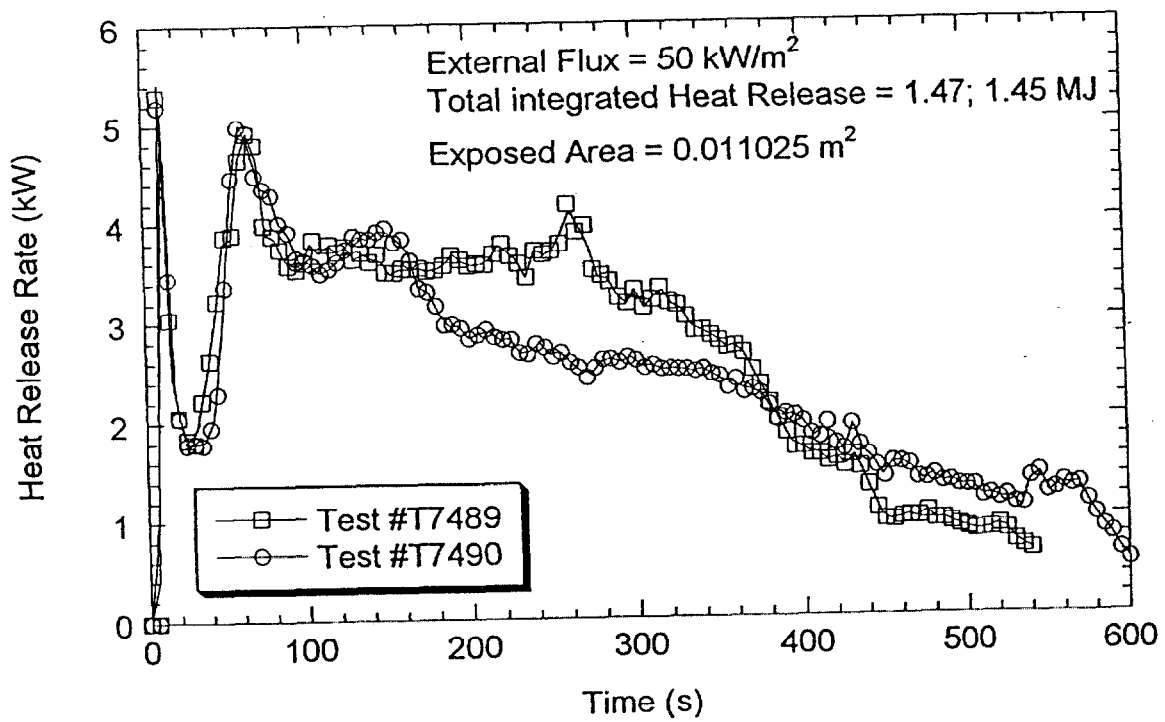
2. The time to flaming ignition of a conditioned sample of corrugated paper as a function of the incident heat flux.



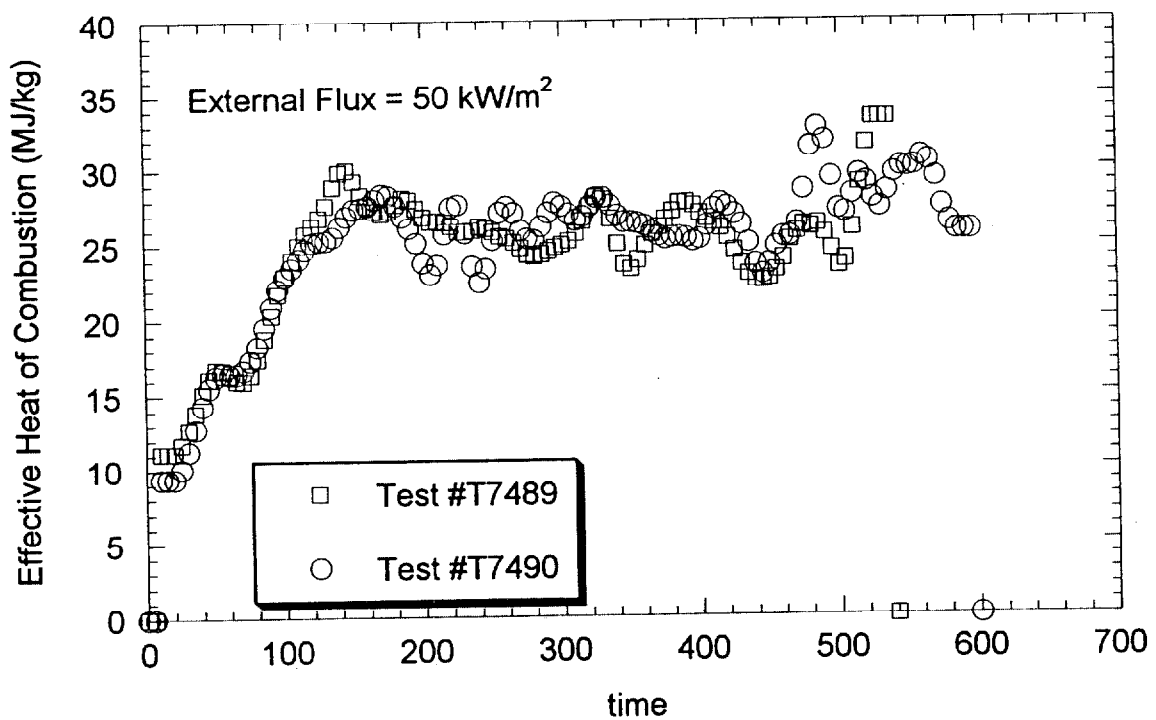
3. The data from Fig. 2 replotted to determine the critical flux.



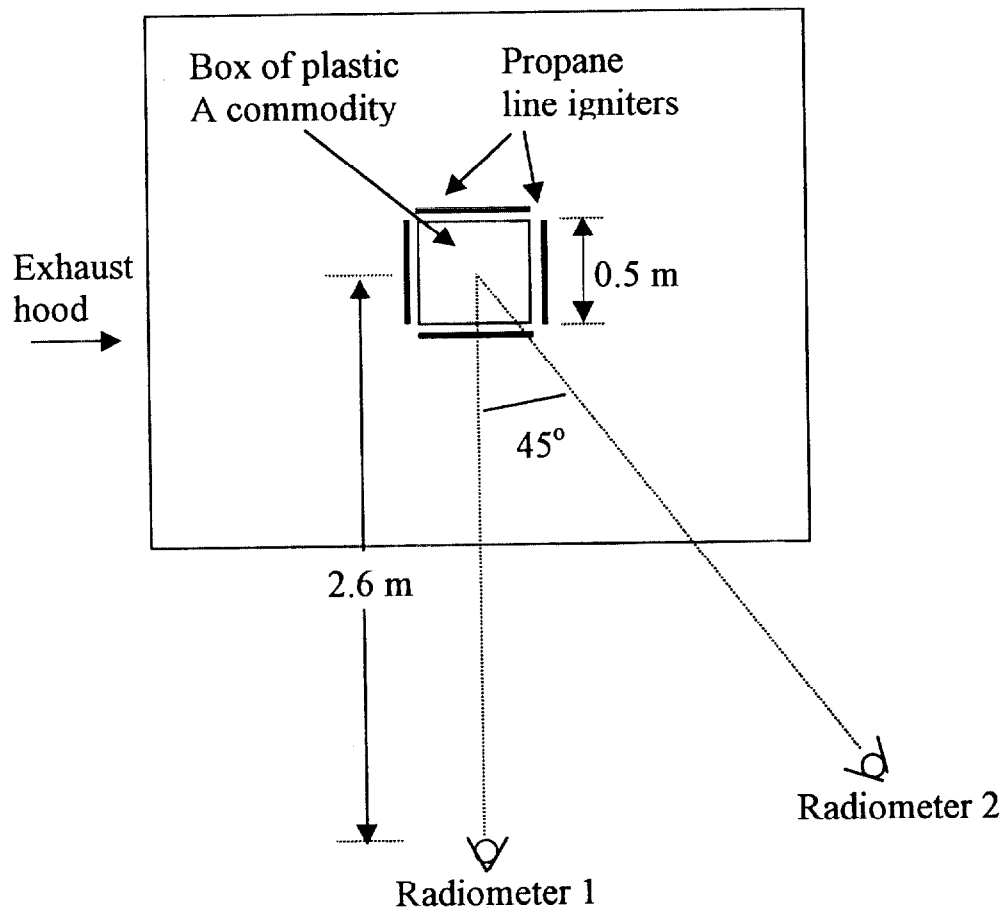
4. The ratio of the critical to the external (or incident) flux as a function of time to ignition.



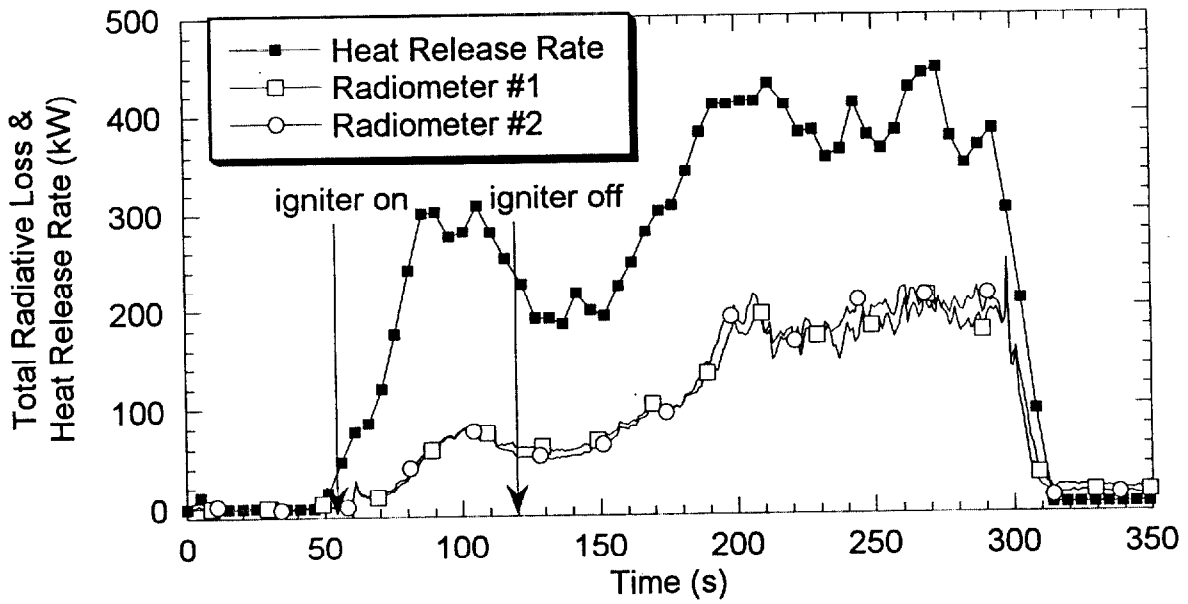
5. The measured heat release rates from two experiments burning single cells of the Group A Plastic Commodity in the cone calorimeter.



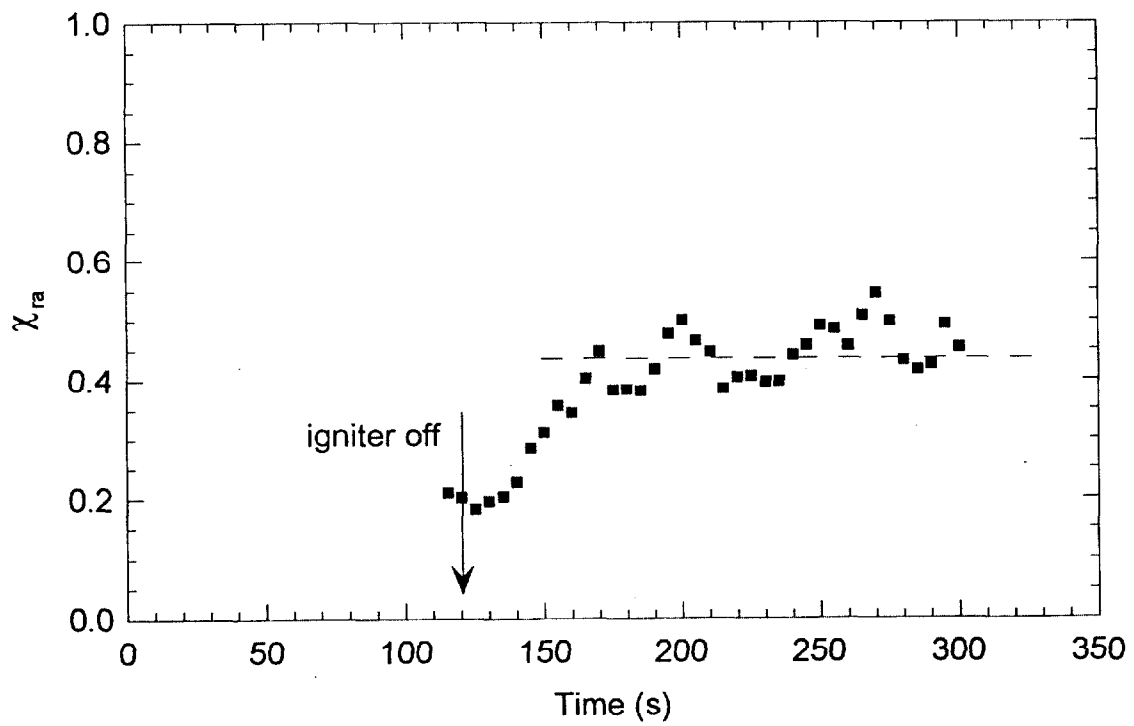
6. The effective heat of combustion ($\chi_a H_c$), which is equal to the ratio of the measured heat release rates to the sample mass loss rate for the same data shown in Fig. 5.



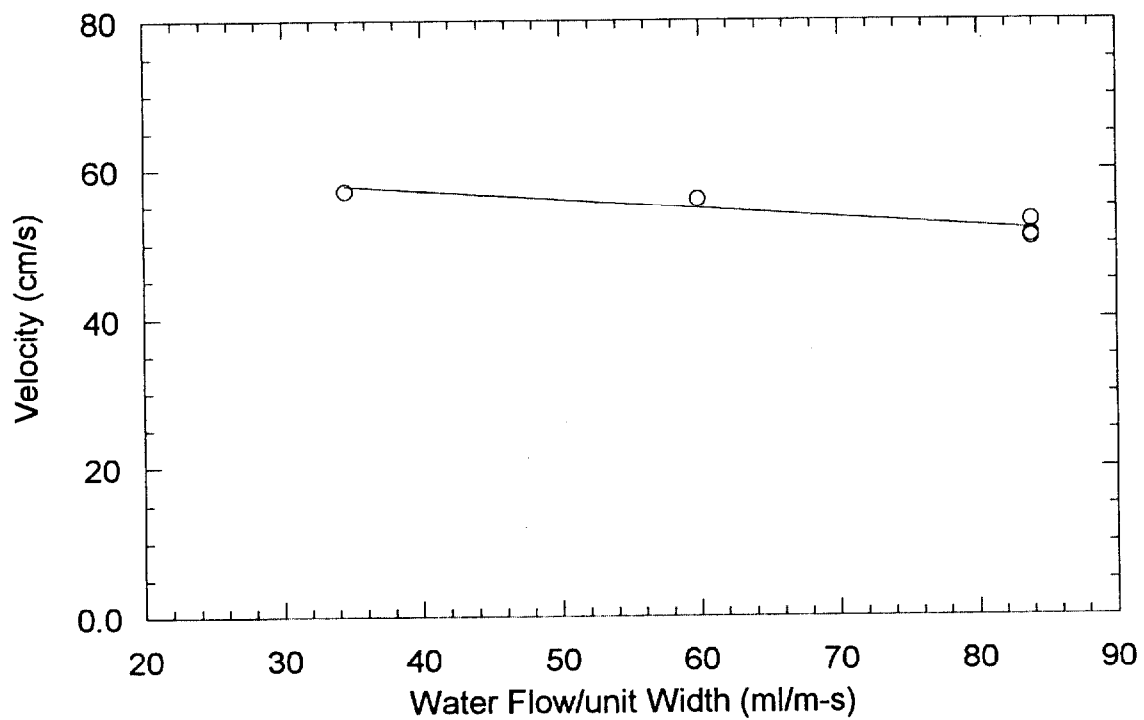
7. A plan-view drawing of the experimental arrangement for the measurement of the effective radiative heat loss fraction of the commodity.



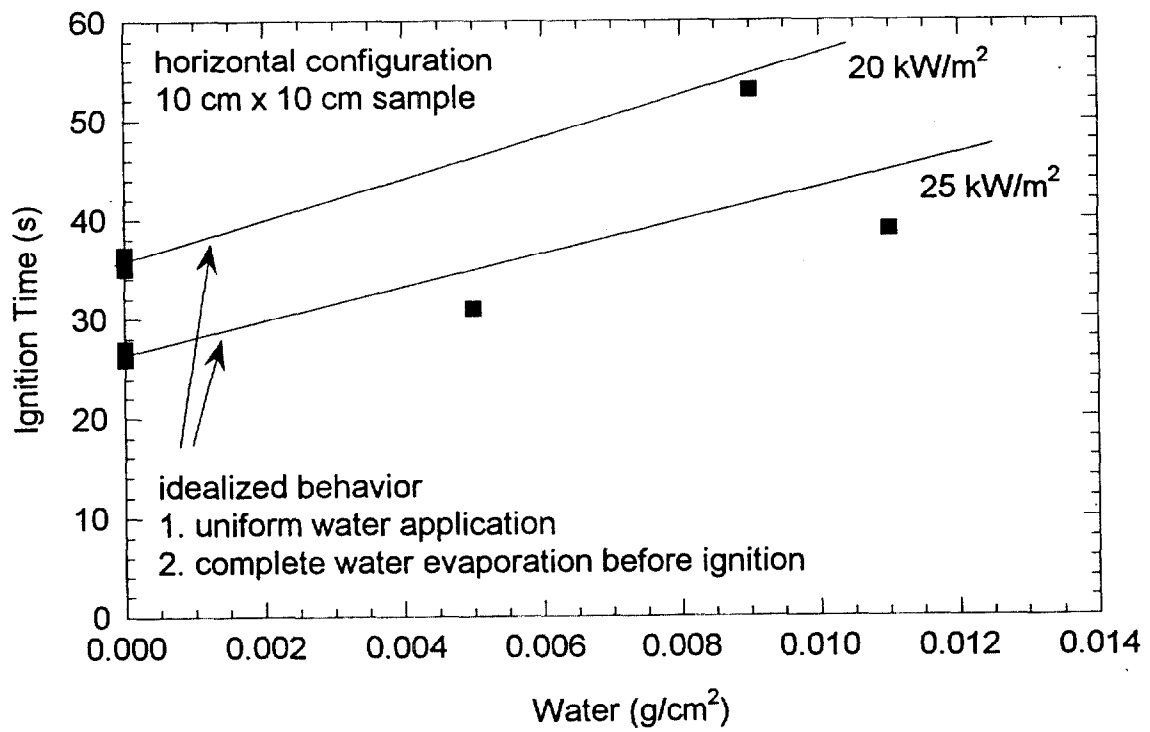
8. The measured total radiative loss (\dot{Q}_r) and the actual heat release rate (\dot{Q}_m) during burning of a single box of commodity.



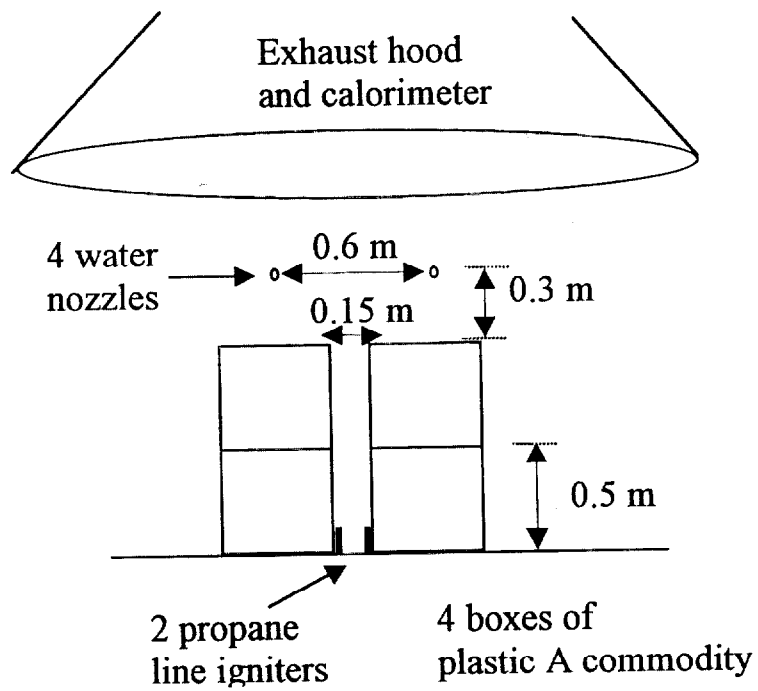
9. The calculated value of χ_{ra} based on the data shown in Fig. 8.



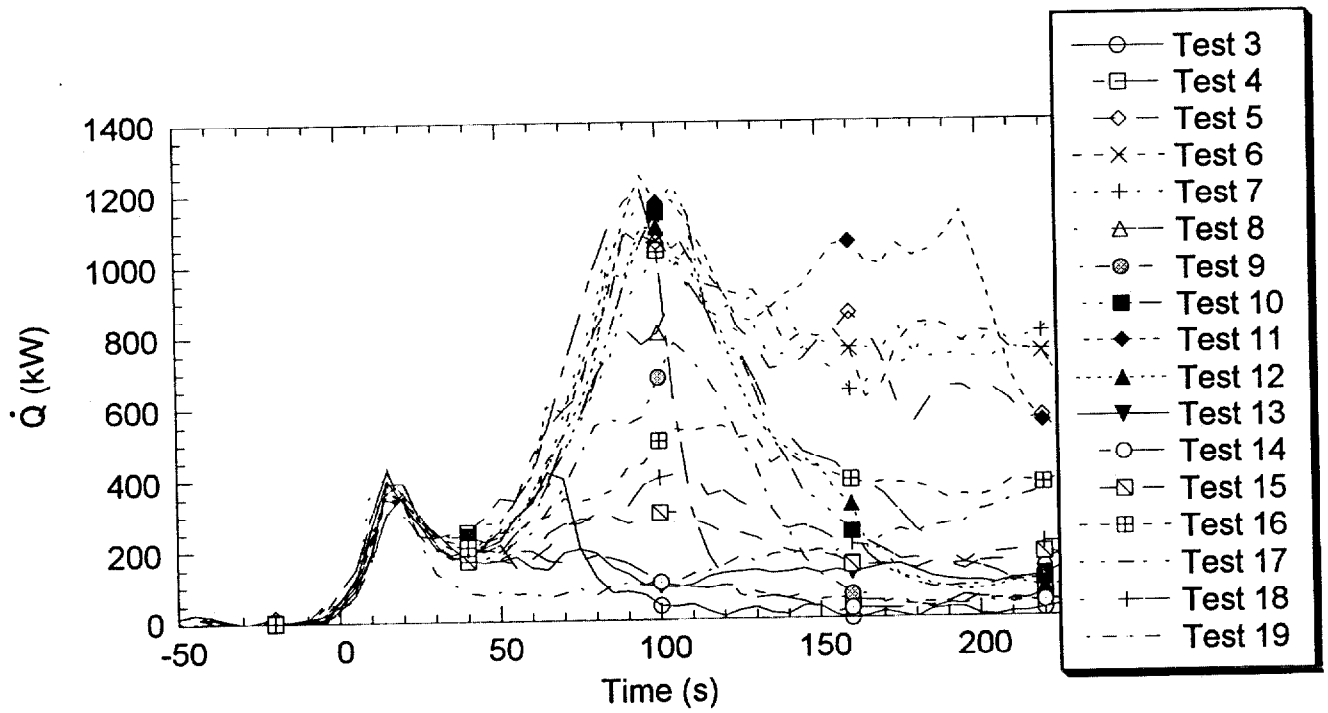
10. The measured water speed and the calculated thickness as a function of the volumetric water flow normalized by the width (=25 cm) of the plate surface.



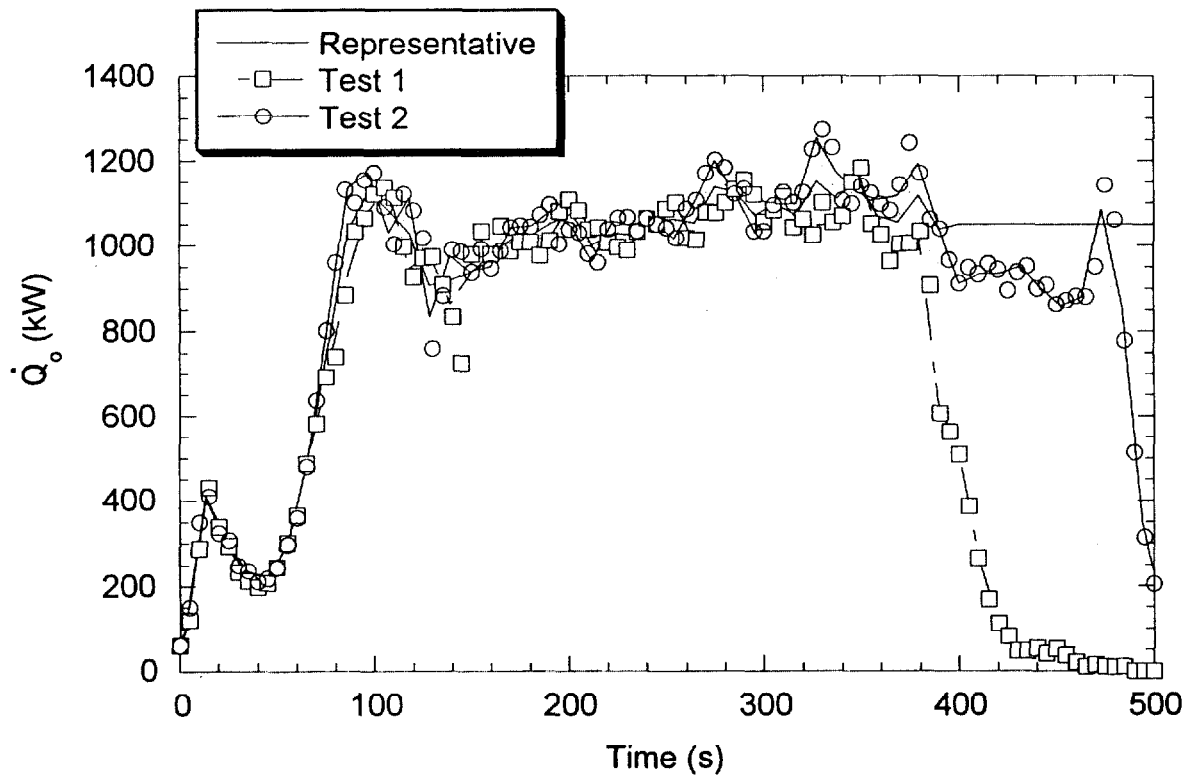
11. The ignition time as a function of the mass of water applied per unit sample area for an incident flux of 20 kW/m² and 25 kW/m².



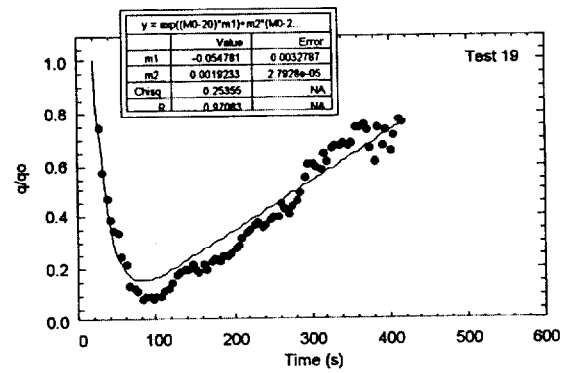
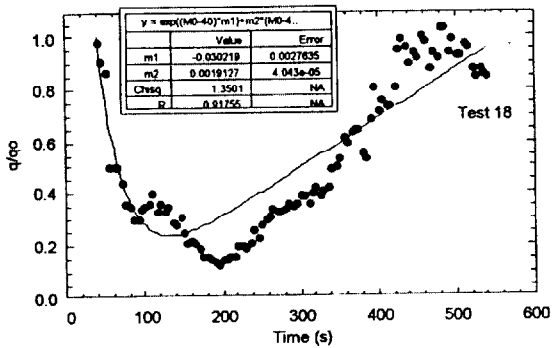
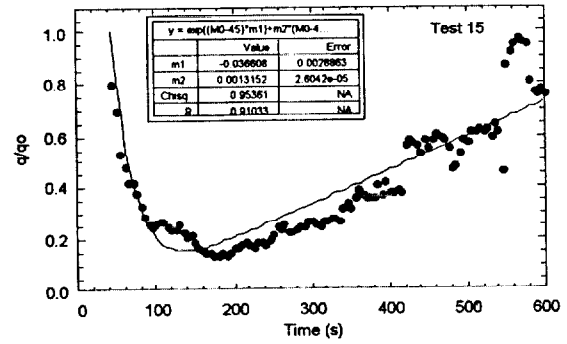
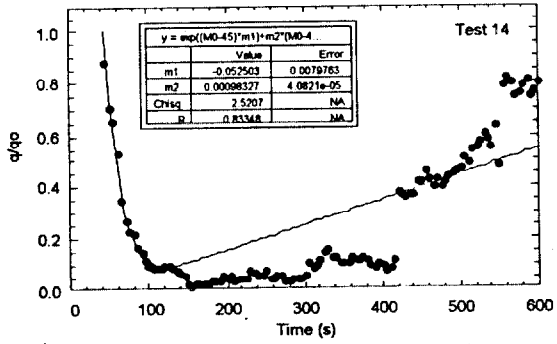
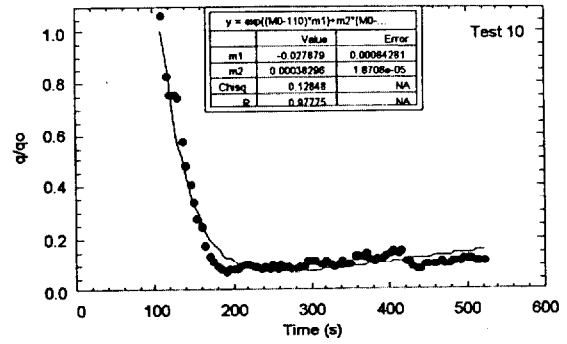
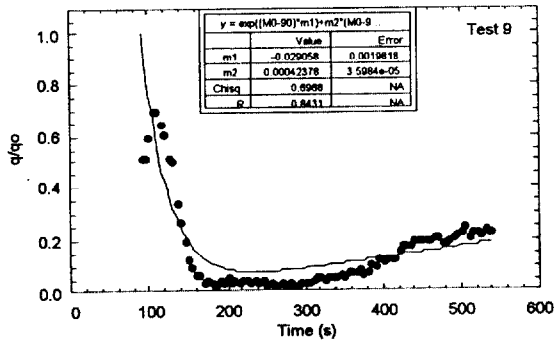
12. The fuel and nozzle arrangement for Tests 1-19.



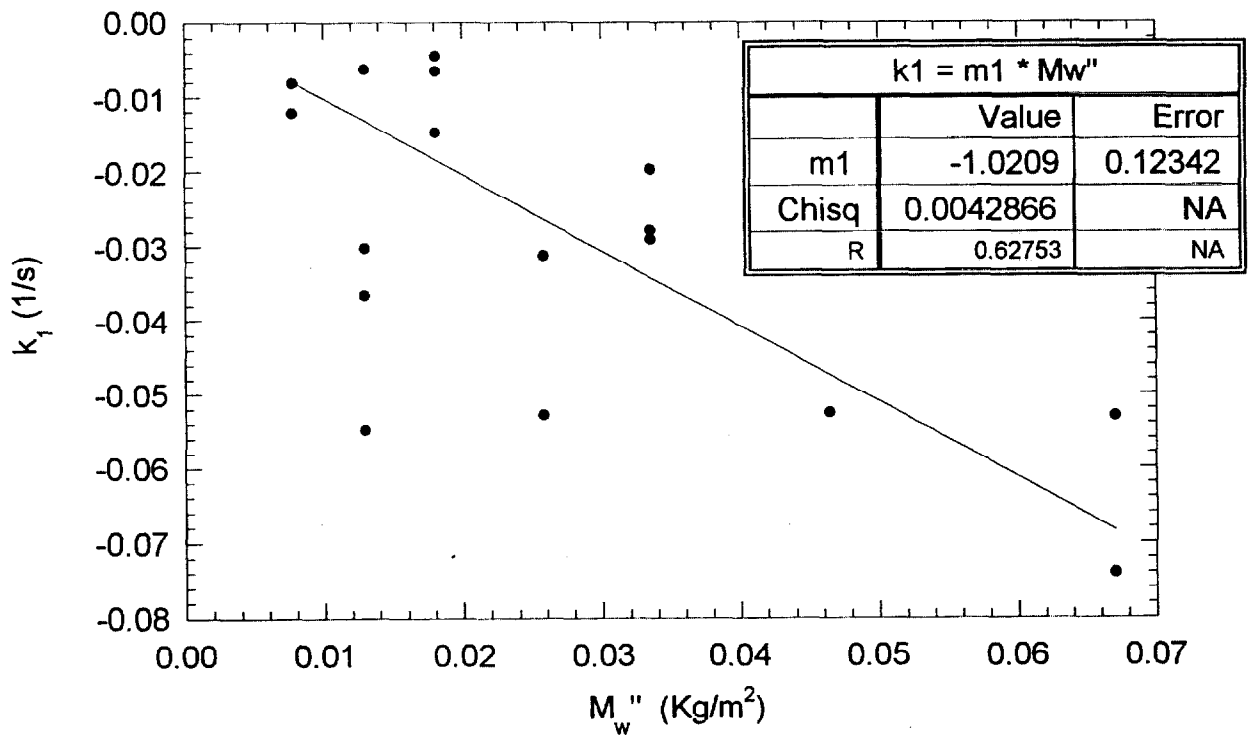
13. The measured heat release rate with water application (\dot{Q}) measured in Tests 3-19.



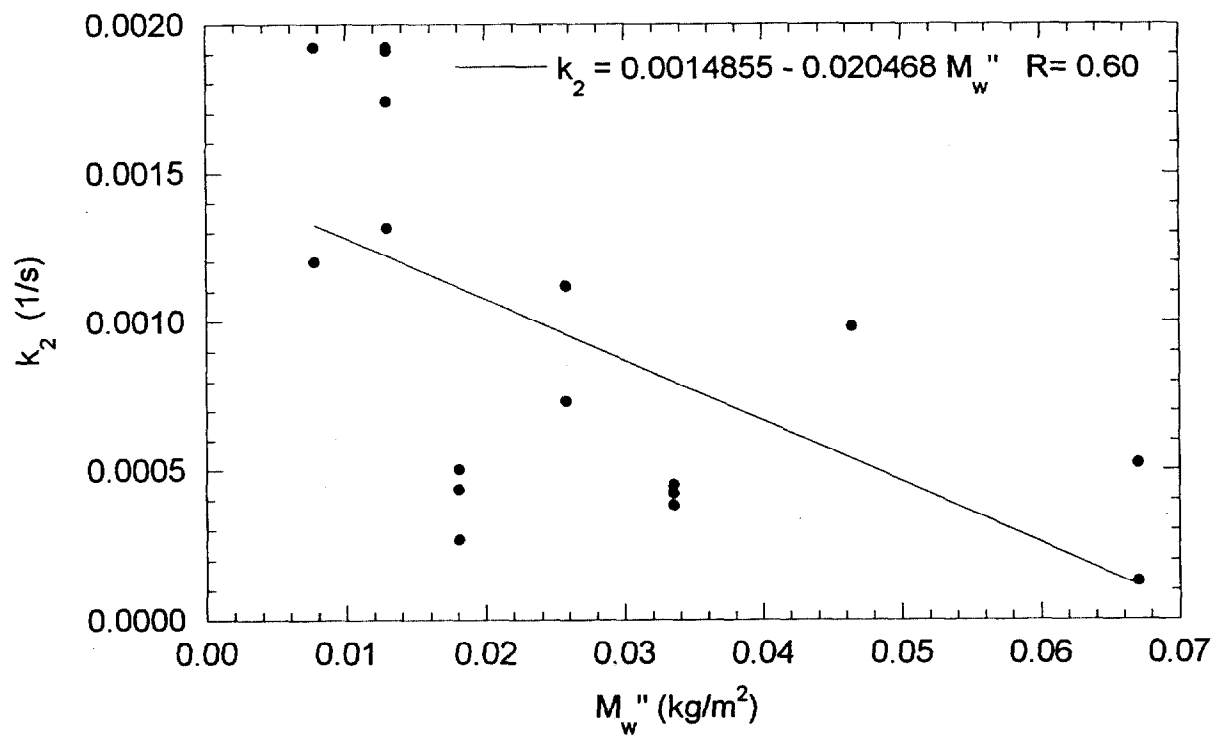
14. The measured heat release rate without water application (\dot{Q}_o) measured in Tests 1 and 2.



15. The normalized heat release rates (\dot{q}''/\dot{q}''_0) and fits using the form given by Eq. 11 for Tests 9, 10, 14, 15, 18, and 19.



16. The value of k_1 as a function of the water application rate (M_w'') for Tests 3-19.



17. The value of k_2 as a function of the water application rate (M_w'') for Tests 3-19.

NIST 114		U.S. DEPARTMENT OF COMMERCE		(ERB USE ONLY)	
		ERB CONTROL NUMBER		DIVISION 864	
		PUBLICATION REPORT NUMBER NISTIR 6439		CATEGORY CODE	
INSTRUCTIONS: ATTACH ORIGINAL OF THIS FORM TO ONE (1) COPY OF MANUSCRIPT AND SEND TO THE SECRETARY, APPROPRIATE EDITORIAL REVIEW BOARD		PUBLICATION DATE November 1999		NUMBER PRINTED PAGES	
TITLE AND SUBTITLE (CITE IN FULL) Reduced-Scale Experiments to Characterize the Suppression of Rack-Storage Commodity Fires					
CONTRACT OR GRANT NUMBER			TYPE OF REPORT AND/OR PERIOD COVERED		
AUTHOR(S) (LAST NAME, FIRST INITIAL, SECOND INITIAL) Hamins, A. and McGrattan, K.			PERFORMING ORGANIZATION (CHECK (X) ONE BOX) <input checked="" type="checkbox"/> NIST/GAITHERSBURG <input type="checkbox"/> NIST/BOULDER <input type="checkbox"/> JILA/BOULDER		
LABORATORY AND DIVISION NAMES (FIRST NIST AUTHOR ONLY) Building and Fire Research Lab, Fire Safety Engineering Division					
SPONSORING ORGANIZATION NAME AND COMPLETE ADDRESS (STREET, CITY, STATE, ZIP)					
PROPOSED FOR NIST PUBLICATION					
<input type="checkbox"/>	JOURNAL OF RESEARCH (NIST JRES)	<input type="checkbox"/>	MONOGRAPH (NIST MN)	<input type="checkbox"/>	LETTER CIRCULAR
<input type="checkbox"/>	J. PHYS. & CHEM. REF. DATA (JPCRD)	<input type="checkbox"/>	NATL. STD. REF. DATA SERIES (NIST NSRDS)	<input type="checkbox"/>	BUILDING SCIENCE SERIES
<input type="checkbox"/>	HANDBOOK (NIST HB)	<input type="checkbox"/>	FEDERAL INF. PROCESS. STDS. (NIST FIPS)	<input type="checkbox"/>	PRODUCT STANDARDS
<input type="checkbox"/>	SPECIAL PUBLICATION (NIST SP)	<input type="checkbox"/>	LIST OF PUBLICATIONS (NIST LP)	<input type="checkbox"/>	OTHER _____
<input type="checkbox"/>	TECHNICAL NOTE (NIST TN)	<input checked="" type="checkbox"/>	NIST INTERAGENCY/INTERNAL REPORT (NISTIR)		
PROPOSED FOR NON-NIST PUBLICATION (CITE FULLY)		<input type="checkbox"/>	U.S.	<input type="checkbox"/>	FOREIGN
		<input checked="" type="checkbox"/>	PAPER	<input type="checkbox"/>	CD-ROM
		<input type="checkbox"/>	DISKETTE (SPECIFY)	OTHER (SPECIFY) _____	
SUPPLEMENTARY NOTES					
ABSTRACT (A 2000-CHARACTER OR LESS FACTUAL SUMMARY OF MOST SIGNIFICANT INFORMATION. IF DOCUMENT INCLUDES A SIGNIFICANT BIBLIOGRAPHY OR LITERATURE SURVEY, CITE IT HERE. SPELL OUT ACRONYMS ON FIRST REFERENCE.) (CONTINUE ON SEPARATE PAGE, IF NECESSARY.)					
<p>A series of experiments are described that investigate the burning and water suppression of rack-storage commodity fires. The objective of the research reported here is to support the NIST Industrial Fire Simulator (IFS), a computational fluid dynamics model. The IFS model predicts fire growth, sprinkler activation, and suppression by water. The model requires appropriate and implementable sub-grid algorithms that adequately represent the full-scale heat and mass transfer that occurs in a warehouse fire.</p> <p>Several types of experiments were conducted. These include ignition measurements using the LIFT apparatus and the cone calorimeter, and heat release rate measurements using oxygen consumption calorimetry. All of these measurements were made with and without water application.</p>					
KEY WORDS (MAXIMUM OF 9; 28 CHARACTERS AND SPACES EACH; SEPARATE WITH SEMICOLONS; ALPHABETIC ORDER; CAPITALIZE ONLY PROPER NAMES)					
burning rate; computer models; fire growth; fire suppression; ignition; sprinklers					
AVAILABILITY			NOTE TO AUTHOR(S): IF YOU DO NOT WISH THIS MANUSCRIPT ANNOUNCED BEFORE PUBLICATION, PLEASE CHECK HERE.		
<input checked="" type="checkbox"/>	UNLIMITED	<input type="checkbox"/>	FOR OFFICIAL DISTRIBUTION - DO NOT RELEASE TO NTIS		
<input type="checkbox"/>	ORDER FROM SUPERINTENDENT OF DOCUMENTS, U.S. GPO, WASHINGTON, DC 20402				
<input checked="" type="checkbox"/>	ORDER FROM NTIS, SPRINGFIELD, VA 22161				

WORDPERFECT